

Viscoelastic characterization of the retracting cytoskeleton using subcellular detachment

Sang-Hee Yoon,^{1,2} Chan Lee,³ and Mohammad R. K. Mofrad^{1,a)}

¹Department of Bioengineering, Molecular Cell Biomechanics Laboratory, University of California, Berkeley, California 94720, USA

²Department of Mechanical Engineering, University of California, Berkeley, California 94720, USA

³Agency for Defense Development, Yuseong P.O. Box 35, Daejeon 305-600, Republic of Korea

(Received 30 July 2010; accepted 25 January 2011; published online 28 March 2011)

Characterization of the cytoskeleton's viscoelastic properties is essential for understanding cellular dynamics in many biological functions of the cell, especially cell migration. The viscoelastic properties of the retracting NIH 3T3 fibroblasts are investigated here to shed light on the mechanics and dynamics of cell migration. A part of the cell is detached by electrochemically desorbing a gold-thiol self-assembled monolayer. The viscoelastic properties of the detached and retracting cytoskeleton are then estimated using time-sequential imaging combined with atomic force microscopy. The retracting cytoskeleton exhibits a threefold decrease in stiffness and a 30-fold increase in viscous damping capacity as compared to those in the adhered (stationary) cytoskeleton. © 2011 American Institute of Physics. [doi:10.1063/1.3556557]

It is known that adherent cells experience a reversible polymerization/depolymerization process during which soluble actin monomers are combined/separated with accessory proteins in the cytoskeleton. This process is key to cell migration. Any irregularity in this phenomenon could undermine the biological functions of a cell, potentially causing serious pathophysiological consequences.¹ The mechanical properties of the cytoskeleton, therefore, must be quantitatively characterized for a better understanding of cellular dynamics.

There have been a variety of methods for measuring the physical properties of a cell: magnetic-particle-based cytometry,² micropipette aspiration,³ optical tweezer,⁴ fluid shear flow method,⁵ cytoindenter,⁶ atomic force microscopy (AFM);⁷ see Ref. 8 for a comprehensive review. These methods were, however, used to characterize the physical properties of the *adhered* (i.e., *stationary*) cell. In this paper, the mechanical properties of the *retracting* (moving) cytoskeleton of NIH 3T3 fibroblasts are measured, along with a continuum mechanical model for the retracting cell (NIH 3T3 cells are mouse embryonic fibroblast cells, where the acronym 3T3 refers to the cell transfer and inoculation protocol for the cell line, and literally means “3-day transfer, inoculum 3×10^5 cells”). Specifically, the viscoelastic properties of these cells are determined from the time-sequential images of cell retraction in conjunction with AFM indentation results.

When a cell migrates, its thin ($\leq 1 \mu\text{m}$) cytoskeletal layer experiences a typical strain profile as shown in Fig. 1(a). The cell extends and adheres to the substrate at $0 \leq t < t_1$; the nucleus translocates at $t_1 \leq t < t_2$; the cell is detached and retracts at $t_2 \leq t$. A standard linear viscoelastic solid model composed of two springs k_1 , k_2 and one dashpot c [Fig. 1(b)] is used here to describe the retraction of a detached cell because it can take into consideration both creep and stress relaxation phenomena. The cytoskeleton is as-

sumed as an isotropic and viscoelastic continuum. At STEP 1 ($0 \leq t < t_2$, relaxation phase), the strain ε profile is expressed as $\varepsilon(t) = \varepsilon_0 H(t)$ where $H(t)$ is a Heaviside function. The initial stress at $t = t_1 \approx 0$ is σ_0 . The stress σ profile, obtained by the Laplace transformation of the stress-strain equation, enables us to find the stress in the cytoskeleton at $t = t_2 \approx \infty$, $\sigma_{t_2} = k_1 k_2 \varepsilon_0 / (k_1 + k_2)$, where k_1 and k_2 represent elastic spring constants in the model (see Fig. 1). At STEP 2 ($t \geq t_2$, creep phase), the stress is assumed as an inverted Heaviside function with a jump of σ_{t_2} at $t = t_2$, $\sigma(t) = \sigma_{t_2} [1 - H(t - t_2)]$. After the Laplace transformation of the stress-strain equation, the strain normalized with respect to ε_0 , is given by (see details in the supplementary materials provided in Ref. 9)

$$\varepsilon^* = \frac{\varepsilon(t - t_2)}{\varepsilon_0} = \left(1 - \frac{k_2}{k_1 + k_2}\right) e^{-k_2/c(t - t_2)}. \quad (1)$$

To acquire the time-sequential images of cytoskeletal retraction, a new biological platform for subcellular detachment [Fig. 2(a)] is microfabricated using optical lithography, e-beam evaporation, and lift-off. It consists of an array of gold electrodes patterned on a Pyrex glass substrate. Each gold electrode is $10 \mu\text{m}$ in width and $3 \mu\text{m}$ in gap. The

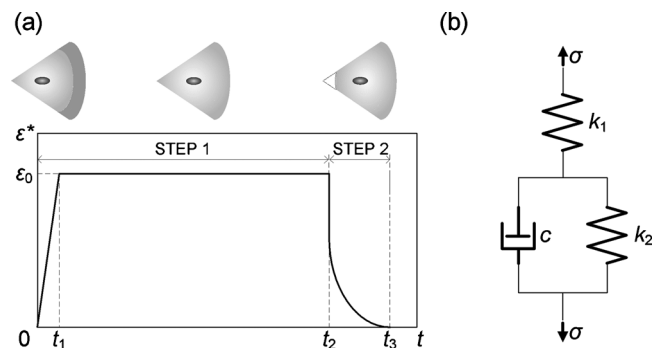


FIG. 1. Cell migration. (a) A typical strain profile in a migrating cell: cell adhesion ($t=0$); cytoskeletal protrusion at the leading edge ($0 < t < t_1$); nucleus translocation ($t_1 \leq t < t_2$); cytoskeletal detachment and retraction at the trailing edge ($t_2 \leq t$). (b) Proposed model of retracting cytoskeleton.

^{a)} Author to whom correspondence should be addressed. Tel.: 510-643-8165. FAX: 510-642-5835. Electronic mail: mofrad@berkeley.edu.

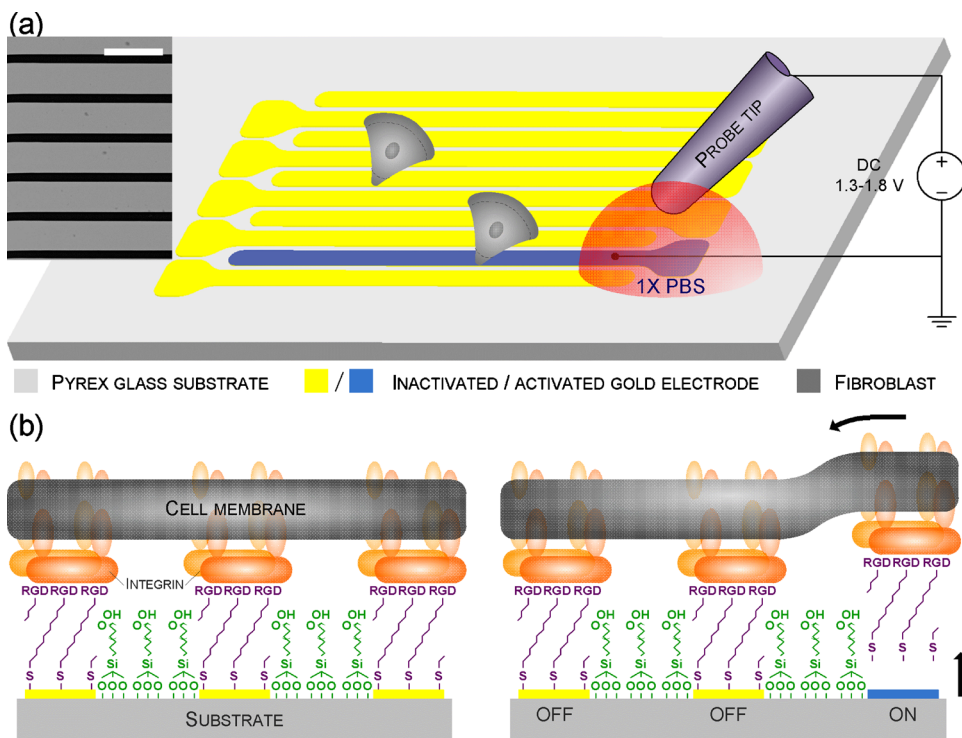


FIG. 2. (Color online) A biological platform for subcellular detachment. (a) Schematic of the biological platform. The scanning electron microscope image of gold electrodes is shown in the inset. Scale bar is 20 μm. (b) Working principle. Before subcellular detachment (left), a RGD binding to integrin of fibroblasts is formed on the gold electrodes functionalized with RGD-terminated thiol but no cell adhesion is made on a polyethylene glycol-coated Pyrex glass substrate. Upon subcellular detachment (right), a part of the cell is detached and in turn retracting.

microfabricated gold electrodes are functionalized with arginine-glycine-aspartic acid (RGD)-terminated thiol to make the electrodes cell-adhesive, whereas the Pyrex glass substrate is coated with polyethylene glycol to achieve a cell-resistant surface (see details of materials and method in supplementary material provided in Ref. 9). An RGD peptide is tethered to the gold electrodes via spontaneous chemisorption of thiol compound, $R-S-H + Au \rightarrow R-S-Au + 1/2H_2$ where R is a substituent. Fibroblasts are loaded into the functionalized biological platform, and the cell adheres to the platform [Fig. 2(b), left]. Upon subcellular detachment [Fig. 2(b), right], the gold-thiol self-assembled monolayer is reductively desorbed with activation voltage of -1.3 to -1.8 V, $R-S-Au + H^+ + e^- \rightarrow R-S-H + Au$.¹⁰ This reaction leads to the detachment and retraction of one part of the cell placed on the activated gold electrode.

Our subcellular detachment experiments for fibroblasts were performed in the CO₂ independent media containing 10% fetal bovine serum (FBS) and 1% penicillin-streptomycin (pen-strep) at 36 °C (see Ref. 9 for further details on materials and methods). An activation signal was produced by a three-electrode system where gold (of the biological platform), platinum, and Ag/AgCl electrodes play as

working, counter, and reference electrodes, respectively. The strain profile of the retracting cytoskeleton [Fig. 3(b)] was acquired from the time-sequential images [Fig. 3(a)] and was normalized with respect to initial strain ϵ_0 . A mathematical expression which has the best fit to the experimental results of 20 fibroblasts was determined as $\epsilon^* = 0.799e^{-0.055t}$ indicating $k_1/(k_1+k_2) = 0.799$ and $k_2/c = 0.055$.

The above two equations were not enough for calculating the three parameters of k_1 , k_2 , and c . The elastic modulus of the retracting cytoskeleton was, therefore, measured with an Autoprobe CP AFM (Park Science Instruments) at a low-speed of 10 nm/s which quantifies the elastic modulus without involving viscous damping. The elastic modulus was determined by measuring the deflection of an AFM tip which slowly indents on the detached cytoskeleton (further details can be found in supplementary material presented in Ref. 9). Before indentations [Fig. 4(a)], the furthestmost end of the protruding cytoskeleton of fibroblasts [indicated by “○” in the inset of Fig. 4(b)] was lightly held with a glass microcapillary (TransferTip-RP, Eppendorf) to prevent the retraction of the detached cytoskeleton after subcellular detachment, followed by AFM indentations [indicated by “+” in the

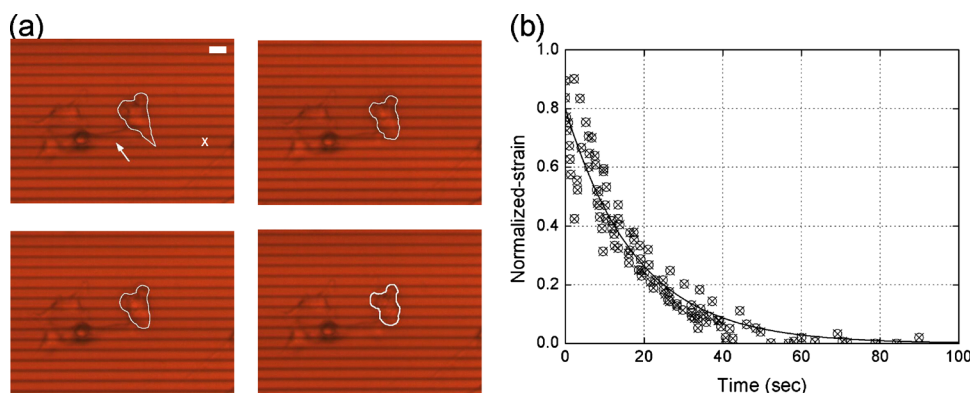


FIG. 3. (Color online) Subcellular detachment. (a) Time-sequential images of the retracting cytoskeleton after subcellular detachment where the gold electrode marked with “x” is activated. Scale bar is 20 μm. (b) Normalized-strain ϵ^* as a function of time t of the retracting cytoskeleton. See text for further details.

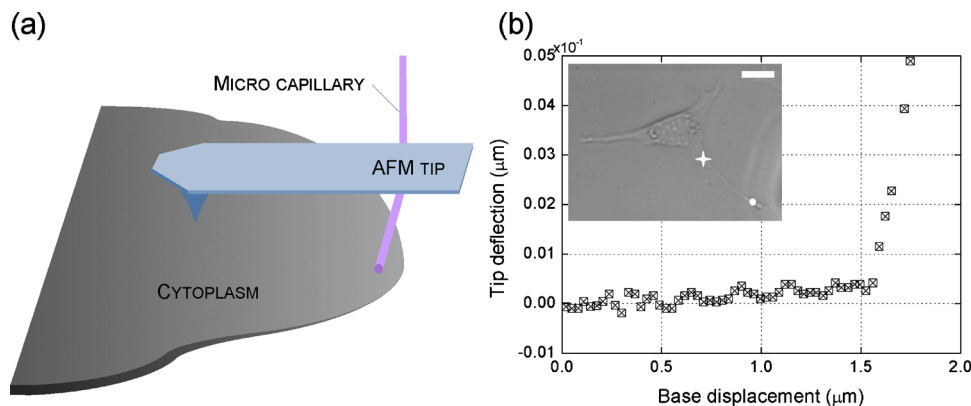


FIG. 4. (Color online) AFM indentation. (a) Experimental setup. (b) Tip deflection as a function of AFM base displacement for the detached cell. The AFM tip is initially located above the cell when the AFM base displacement is zero. The AFM indentation is performed with decreasing the distance between AFM tip and cell (moving to the right along the plot). The symbols of + and \circ are indentation and cell-holding positions, respectively. Scale bar is 20 μm .

inset of Fig. 4(b)]. After 24 h of cell loading, all indentations were carried out in the CO_2 independent media with 10% FBS and 1% pen-strep at a chamber whose temperature is maintained at 36 $^\circ\text{C}$.

The tip deflection as a function of AFM base displacement for the retracting subcellular region [Fig. 4(b)] shows the elastic modulus [$k_{\text{total}} = k_1 k_2 / (k_1 + k_2)$] is about 1320 ± 310 Pa, averaged from ten measurements. The indentation results were combined with the above normalized-strain profile so that k_1 , k_2 , and c of the retracting cytoskeleton of fibroblasts were determined as 6567 Pa, 1652 Pa, and 300 37 Pa s, respectively. Compared to the previous results^{7,11} of $k_{\text{total}} > 4000$ Pa and $c < 100$ Pa s obtained for the stationary fibroblast cells, the retracting cytoskeleton showed a threefold decrease in elastic modulus and a 30-fold increase in damping coefficient. These results suggest that a retracting cytoskeleton may become softer, and consequently has remarkable increase in damping coefficient after a few seconds of subcellular detachment. This phenomenon is likely owing to the gel-sol transition of actin filaments at subcellular detachment which changes the viscoelastic properties of the retracting cytoskeleton of fibroblasts. At subcellular detachment, the cross-linked network of actin filaments (coupled to focal adhesion) is likely depolymerized in the retracting cytoskeleton. Therefore, the stiffness of the cytoskeleton decreases while its viscous damping capacity increases.

In conclusion, this is the first report to measure the viscoelastic properties of the retracting cytoskeleton of 3T3 fibroblasts. The experimental results demonstrate that our method, combining the time-sequential images of subcellular retraction with AFM indentation experiments, can measure the viscoelastic properties of the moving cytoskeleton, offering better insight on cellular dynamics.

Financial support by the National Science Foundation through CAREER Award (CBET 0955291) is gratefully acknowledged.

¹A. J. Ridley, M. A. Schwartz, K. Burridge, R. A. Firtel, M. H. Ginsberg, G. Borisy, J. T. Parsons, and A. R. Horwitz, *Science* **302**, 1704 (2003).

²A. R. Bausch, W. Möller, and E. Sackmann, *Biophys. J.* **76**, 573 (1999).

³F. Guilak, J. R. Tedrow, and R. Burgkart, *Biochem. Biophys. Res. Commun.* **269**, 781 (2000).

⁴C. T. Lim, M. Dao, S. Suresh, C. H. Sow, and K. T. Chew, *Acta Mater.* **52**, 1837 (2004).

⁵D. P. Theret, M. J. Levesque, M. Sato, R. M. Nerem, and L. T. Wheeler, *J. Biomech. Eng.* **110**, 190 (1988).

⁶D. Shin and K. Athanasiou, *J. Orthop. Res.* **17**, 880 (1999).

⁷H. Haga, S. Sasaki, K. Kawabata, E. Ito, T. Ushiki, and T. Sambongi, *Ultramicroscopy* **82**, 253 (2000).

⁸M. R. K. Mofrad, *Annu. Rev. Fluid Mech.* **41**, 433 (2009).

⁹See supplementary material at <http://dx.doi.org/10.1063/1.3556557> for viscoelastic theory and further details on our experimental materials and methods.

¹⁰C. A. Widrig, C. Chung, and M. Porter, *J. Electroanal. Chem. Interfacial Electrochem.* **310**, 335 (1991).

¹¹H. Haga, M. Nagayama, and K. Kawabata, *Curr. Nanosci.* **3**, 97 (2007).